Gaussian-Shaped Gain-Dopant Distributed Fiber for High Output Power Fiber Amplifier

Zhilun Zhang, Xianfeng Lin, Gui Chen, Lei Liao, Yingbin Xing, Haiqing Li, Jinggang Peng, Nengli Dai, and Jinyan Li

***Abstract*—The remarkable evolution of ytterbium-doped fiber (YDF) lasers and amplifiers is interrupted by a limiting thermo-optical effect called transverse mode instability (TMI). Hereon, we propose a Gaussian-shaped gain-dopant distributed (GSGDD) YDF, which is fabricated by a modified chemical vapor deposition (MCVD) process combined with solution doping technique (SDT). By regulating the solution concentrations of soot layers, the content of Yb^{3+} ions presents Gaussian-shaped distribution in the transverse direction while the refractive index profile (RIP) exhibits a stepped profile. The laser performance of this fiber is verified by a bidirectional pumped master oscillator power amplifier (MOPA). Over 3 kW near-single-mode laser output is obtained with the slope efficiency of 84.9%. At the highest power output, there are no Stokes light components in the spectrum and the beam quality M^2 factor is ∼1.45 These results suggest that the GSGDD fiber owns great potential to achieve high power output with excellent beam quality.**

***Index Terms*—Fiber lasers, doped fiber amplifiers. transverse mode instability.**

I. Introduction

Yb-DOPED fiber lasers have been widely applied to industrial processing, medical treatment, 3D printing, and military defense owing to the high conversion efficiency, efficient heat dissipation, compactness, and good beam quality [1]–[7]. The output power of fiber lasers has been unprecedentedly improved, however, nonlinear effects such as stimulated Raman scattering (SRS) emerge when the peak power exceeds a certain threshold, leading to energy transfer to other wavelengths [1]. By enlarging the mode field area of the gain fiber, the SRS threshold is significantly improved. Nevertheless, in the large mode area (LMA) fibers, more high order modes (HOMs) will be bounded in the fiber core, which may trigger transverse mode instability (TMI) [8] and result in beam quality deterioration. Since the TMI phenomenon was discovered in 2010, it has become the dominant limitation for further power scaling of Yb-doped fiber lasers. TMI appears when the output power exceeds a certain threshold, with beam profile transforming from a stable fundamental mode (FM) into an unsteady mode [9]. The energy coupling between different modes on the time scale of millisecond will lead to a sudden degradation in beam quality [10]–[14]. The TMI threshold will be improved by reducing the core V value [15], increasing the inner cladding diameter [16], employing new fiber structures [17], and controlling the gain dopant distribution in fiber core [18]–[20], etc.

Controlling the gain dopant distribution is an effective way for fiber lasers to enlarge the output power and improve the beam quality [21]–[25]. Confined-doped fiber, by confining the Yb^{3+} ions doping within a smaller diameter in the center of fiber core, makes FM obtain more gain while suppressing HOM [21], [22]. In the early stage of TMI observation, confined doping had been predicted as a possible way to improve the TMI threshold, due to its preferential gain effect [9]. Soon, theoretical simulations suggested that confined doping could efficiently reduce the nonlinear coupling constants of LP01 and LP11 modes and then mitigate TMI [12], [14]. Recently, researchers calculated the TMI threshold of four fiber structures, including confined-doped fiber, etc. The simulation results showed that the TMI threshold of confined-doped fiber was ∼1230 W with a core diameter of 30 μm which was the highest among four fibers [26]. In terms of experimental investigations, confined-doped fiber was utilized for a tandem-pump fiber amplifier, which realized 4 kW laser output with the beam quality M^2 factor of 1.59 [25]. Lately, a 33/400 μm confined-doped fiber was fabricated with Yb^{3+} ions doping diameter ratio of 70%, and it was demonstrated that the TMI threshold of confined-doped fiber was about 1250 W which was 1.74 times that of conventional fiber [20].

In contrast with confined-doped fiber, the GSGDD fiber is another novel type of controlling the gain dopant distribution, whose gain dopant concentration always changes rather than confining the doping region. The doping profile of Yb^{3+} ions presents Gaussian-shaped distribution, and the refractive index profile (RIP) is still stepped [22]. Therefore, the gain dopant profile is designed to more effectively overlap the FM gain field. Originally, researchers calculated the differential-gain ratio of GSGDD fiber with different Gaussian widths. The results showed that Gaussian-shaped gain dopant distribution exhibited similar advantages to confined doping, meanwhile possessing high modal discrimination [23]. However, there is a lack of experimental investigation on it. It is worthy to demonstrate the laser properties such as TMI performance and beam quality of GSGDD fiber in high power fiber laser system.

In this study, we propose a Gaussian-shaped gain-dopant distributed (GSGDD) fiber fabricated by MCVD process combined with SDT for the first time, whose core and inner cladding

Manuscript received June 8, 2021; revised July 7, 2021; accepted July 9, 2021. Date of publication July 14, 2021; date of current version September 3, 2021. This work was supported by the National Natural Science Foundation of China under Grants 61975061 and 61735007. *(Corresponding author: Yingbin Xing.)*

The authors are with the Wuhan National Laboratory for Optoelectronics, Huazhong University of Science and Technology, Wuhan 430074, China (e-mail: zzl0910@hust.edu.cn; lxf1210@hust.edu.cn; chen_gui@hust.edu.cn; liaolei5020@hust.edu.cn; xingyb@hust.edu.cn; lhq@mail.hust.edu.cn; jgpeng@mail.hust.edu.cn; dainl@hust.edu.cn; ljy@mail.hust.edu.cn).

Digital Object Identifier 10.1109/JPHOT.2021.3096716

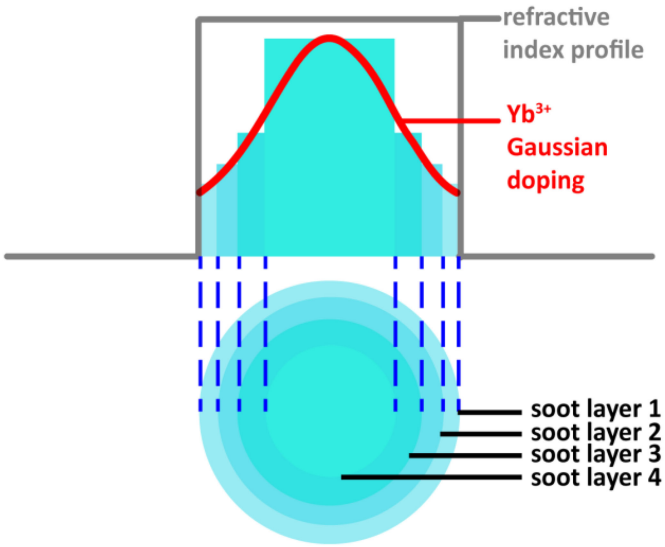

Fig. 1. Designed Yb3+ ions distribution in GSGDD fiber core.

diameters are 32 μm and 400 μm, respectively. The Yb^{3+} ions present Gaussian distribution with a Gaussian width of 16.9 μm, owing to different gain dopant concentrations in each soot layer, and simultaneously, RIP is still stepped. The laser performances, especially TMI effect and beam quality, are investigated in detail by constructing a bidirectional-pumping fiber amplifier. Finally, we realize 3 kW near-single-mode laser output without SRS, and the beam quality maintains stable in the whole experiment.

II. Fiber Design and Fabrication

Generally speaking, the difficulties in fabricating GSGDD fiber were that, on the one hand, gain dopant distribution presented Gaussian shape in the fiber core, on the other hand, the RIP exhibited nearly stepped profile. To put it simply, we just needed to dope different concentrations of Yb^{3+} ions in each soot layer, making it present Gaussian-shaped distribution, and meanwhile, adjust the concentrations of other ions to ensure the equal refractive index difference (RID). To make the distribution of Yb^{3+} ions closer to Gaussian shape, in theory, the more soot layers we deposited, the more precise Gaussian distribution we could obtain. However, plenty of soot layers would greatly increase the fabrication difficulties and cost. On the contrary, a few soot layers deposition could also obtain Gaussian-shaped gain-dopant distribution owing to ions diffusion effect. The designed diagram of the GSGDD fiber core was shown in Fig. 1, four soot layers were deposited, and the fitted Gaussian-shaped curve was also exhibited in the solid red line. For sufficient pump absorption while prevent excessive Yb^{3+} concentration resulting in Yb^{3+} clustering, the concentrations of Yb_2O_3 increased from 0.05 mol% to 0.15 mol% along soot layers, which were determined according to the Gaussian curve. Moreover, Al_2O_3 was doped into the SiO_2 matrix, which Al^{3+} ions were advantageous to improve the solubility of rare earth ions and eliminate crystallization [27]. To effectively restrain photodarkening (PD) effect, Ce^{3+} ions were co-doped into the SiO_2 matrix [28], and it could greatly improve the PD resistivity without obvious disadvantageous influence on the laser performance [29]. The above elements had positive refractive index contributions and would increase numerical aperture (NA). In order to appropriately decrease the fiber core NA, F^- ions were doped into fiber core owing to its negative refractive index [30].

Further, the concentrations of several ions should be earnestly discussed. The contributions of all the doped ions for refractive index increment of GSGDD fiber core can be expressed as:

$$\Delta n \times 10^4 = 67\mathrm{C}_{\mathrm{Yb_2O_3}} + 23\mathrm{C}_{\mathrm{Al_2O_3}} + 67\mathrm{C}_{\mathrm{Ce_2O_3}} - 50\mathrm{C}_{\mathrm{SiF_4}}.$$

The NA of overall fiber core was designed to be ~0.06. The concentrations of the doping components Yb_2O_3, Al_2O_3, Ce_2O_3, and SiF_4 were carefully designed and specifically given in Table 1. It could be found that Yb_2O_3 significantly increased from soot layer 1 to soot layer 4, which made the gain dopant profile as close to Gaussian shape as possible. The Al_2O_3 gradually decreased to balance the RID. The contents of Ce_2O_3 and SiF_4 were not high and they basically maintained constant along the radial direction of the fiber core. Moreover, Al_2O_3 itself was very high and properly regulating its solution concentration could easily balance the RID.

The next step was the fabrication of GSGDD fiber preform based on the above consideration, including deposition and pre-sintering of soot layers, solution soaking, dehydration, vitrification and collapsing into preforms. After several technological explorations, we fabricated a preform that aligns with our design parameters. As shown in Fig. 2(a), a flat refractive index profile for fiber core without any center dip or peak and an ideal index match were obtained. The RID and NA of fiber core were 0.0012 and 0.061, respectively. After that, the fabricated preform was milled into an octagonal shape, and then drawn and coated with polymer coatings on a drawing tower to form a double-clad fiber, whose cross-sectional microscopic image was also attached to Fig. 2(a). The octagonal inner cladding was beneficial to improve pump absorption, while the circular core was better to match the passive fiber. The distributions of Yb^{3+}, Al^{3+}, Ce^{3+}, and F^- across fiber core were characterized by electron probe microanalysis (EPMA) and shown in Fig. 2(b). On account of the diffusion of Yb^{3+} ions, the doping profile was nearly Gaussian type with a Gaussian width of 16.9 μm. The distribution of Al^{3+} represented the core diameter with 32 μm. Besides, the pump absorption coefficient of GSGDD fiber was measured to be 1.07 dB/m at 976 nm.

III. Experimental Setup

The experimental setup of the master oscillator power amplifier (MOPA) is depicted in Fig. 3. The MO consisted of high reflectivity fiber Bragg grating (HR-FBG), active fiber, and output coupler fiber Bragg grating (OC-FBG). The reflectivity of HR-FBG and OC-FBG at 1080 nm were ~99% and ~10%, respectively. The active fiber used a commercial 20/400 μm Yb-doped double-clad fiber, with the core and cladding NA of 0.065 and 0.46, respectively. Six laser diodes (LDs) with a center wavelength of 976 nm were combined by a 7 × 1 pump combiner (PC) and injected into the resonant cavity to generate laser. After coupled output by OC-FBG and stripped by cladding light stripper (CLS), the seed light with the center wavelength of 1080.18 nm and output power of 100 W injected into the PA

TABLE 1
THE DESIGNED CONCENTRATION OF Yb_2O_3, AL_2O_3, Ce_2O_3 AND SiF_4 IN SOOT LAYER 1, 2, 3 AND 4

Soot layer	C(Yb_2O_3) mol%	C(Al_2O_3) mol%	C(Ce_2O_3) mol%	C(SiF_4) mol%	△ n (10^{-3})	Thickness (μm)
1	0.05	0.73	0.02	0.19	~1.2	4
2	0.064	0.69	0.02	0.19	~1.2	4.8
3	0.085	0.63	0.02	0.19	~1.2	6.2
4	0.15	0.41	0.03	0.19	~1.2	15

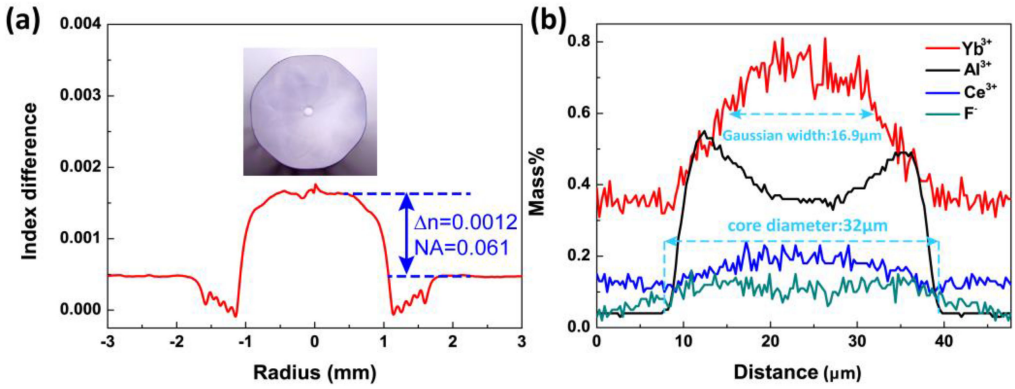

Fig. 2. (a) Refractive index profile and cross-sectional microscopic image; (b) Elemental distribution in GSGDD fiber core.

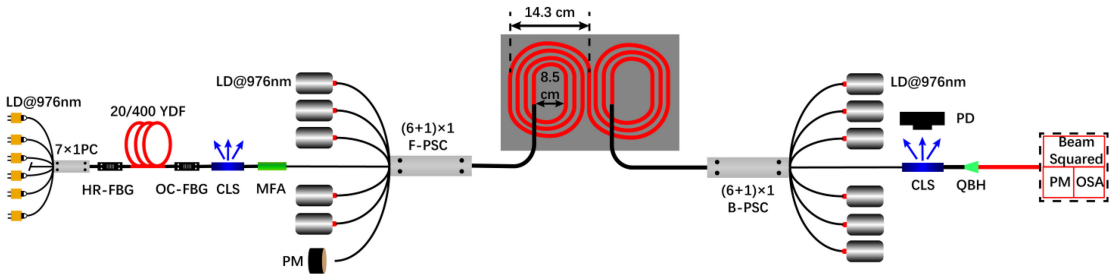

Fig. 3. Scheme of the experimental setup. LD: laser diode, PC: pump combiner, HR- and OC-FBG: high reflectivity- and output coupler fiber Bragg grating, YDF: Yb-doped fiber, CLS: cladding light stripper, MFA: mode field adapter, PM: power meter, F- and B-PSC: forward- and backward- pump and signal combiners, PD: photodetector, QBH: quartz block holder; OSA: optical spectrum analyzer.

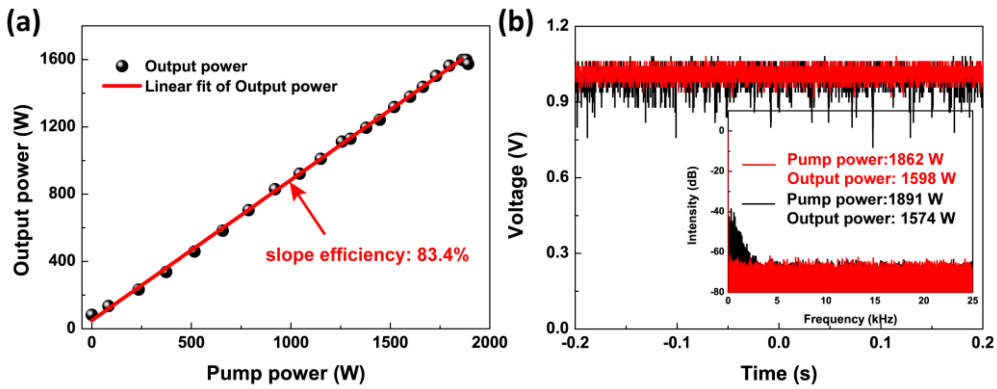

Fig. 4. Experimental results of co-pumping scheme. (a) Output powers at different pump powers; (b) Time and frequency domains at output power of 1598 W and 1574 W.

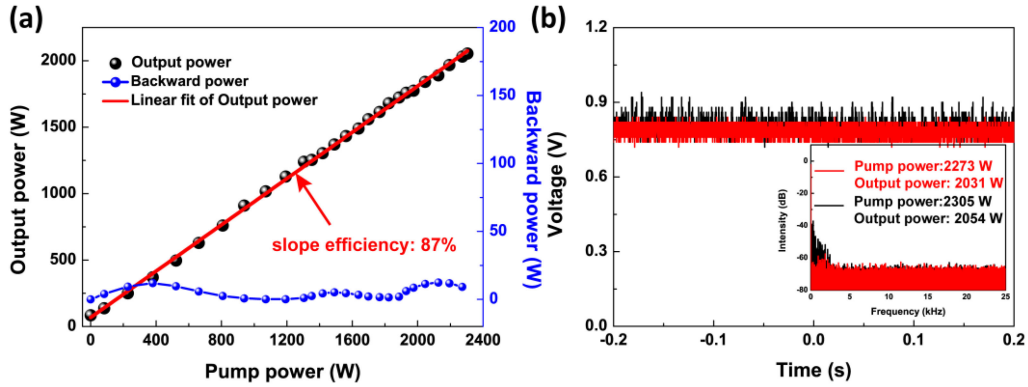

Fig. 5. Experimental results of counter-pumping scheme. (a) Output powers and backward powers at different pump powers; (b) Time and frequency domains at output power of 2031 W and 2054 W.

after passing through mode field adapter (MFA). The signal fiber core and cladding diameters of the co-pumping combiner were 25 μm and 250 μm, respectively, and the output fiber core and cladding diameters were 25 μm and 400 μm, respectively. The signal fiber core and cladding diameters of the counter-pumped combiner were 30 μm and 250 μm, respectively, and the output fiber core and cladding diameters were 30 μm and 400 μm, respectively. Each 976 nm LD could provide pump power up to ~700 W. The above-mentioned fiber was coiled in a water-cooled plate with minimum and maximum bending diameter of 8.5 cm and 14.3 cm, respectively. On account of the unstable pump wavelength, the fiber length of 28 m was utilized for compensating the inadequate pump absorption.

Afterwards, the amplified laser propagated through CLS to strip the cladding light, and the scattered light was received by the photodetector (PD) to collect the time-domain signal and monitor the TMI process. Finally, the laser exported through the quartz block holder (QBH), and its output power, beam quality, and spectrum were measured by a power meter (PM), a beam quality analyzer, and an optical spectrum analyzer (OSA), respectively. Besides, all fibers and heat-produced devices were cooled by 20 °C water.

IV. Results and Discussions

For a start, the pump light from co-pumping source was injected to the amplification stage. The output power versus pump power was shown in Fig. 4(a). And then, we linearly fitted the output power, with the slope efficiency of 83.4%. After output power reaches 1598 W, it began to drop along with further improvement of pump power due to the TMI effect. To determine the TMI threshold of the co-pumping structure, the time and frequency domains at the output power of 1598 W and 1574 W were analyzed, as shown in Fig. 4(b). The fluctuations in time and frequency domain indicated the onsets of TMI. The results showed that the time-domain signal was stable at the output power of 1598 W. However, with further enhancement of pump power, a mass of fluctuations occurred in time and frequency domains. Thus, we considered that the TMI threshold of the co-pumping structure was about 1598 W, and further power scaling was limited by TMI.

Then, the pump light from counter-pumping source was injected to the amplification stage. The output power and backward power versus pump power are shown in Fig. 5(a). The results showed that the slope efficiency of signal laser was 87% and the remanent pump power monitored by PM was always less than 15 W, indicating sufficient pump absorption. Fig. 5(b) showed the time and frequency domains at the output power of 2031 W and 2054 W, which reflected some differences. When the output power exceeded 2031 W, the signals of time and frequency domains began to fluctuate. Therefore, the TMI threshold of the counter-pumping scheme was about 2031 W at this time, and further power scaling was limited by TMI.

Finally, the pump lights from co-pumping and counter-pumping source were corporately injected to the amplifier stage. The output power and backward power versus pump power were shown in Fig. 6(a). In terms of the bidirectional pump, the output power increased with the pump power. The slope efficiency was linearly fitted to 84.9%, and the maximum backward optical power did not exceed 15 W. The onsets of TMI were reflected in a sharp increase of the standard deviations (STD). As shown in Fig. 6(b), the values of STD at 2950 W and 3015 W 3048 W were 0.0217 and 0.0216, 0.0777, respectively. Hence, the STD value increased sharply during the output power enlarged from 3015 W to 3048 W. When the output power reached 3015 W, the time-domain signal slightly fluctuated. After fast Fourier transform (FFT) analysis, there was a mass of independent peaks in its Fourier spectrum, as shown in Fig. 6(c). At this moment, the TMI threshold was about 3015 W. The laser spectrums at several output powers were shown in Fig. 6(d). The 3 dB linewidth gradually widened from 0.7 nm of the seed light to 3.98 nm of 3015 W. No Stokes light components existed in whole experiments.

The beam quality M^2 factors were also measured and shown in Fig. 7, which almost remained constant. The beam qualities at seed power of 83 W and output power of 3015 W were specifically shown in Fig. 8(a) and (b), respectively. The beam quality M^2 factor at seed power of 83 W was $M_x{}^2 = 1.436$, $M_y{}^2 = 1.452$. At the output power of 3015 W, the M^2 factor was $M_x{}^2 = 1.481$, $M_y{}^2 = 1.422$. Due to the gradual increase of output power, the focal distances of the imaging lens slightly changed, resulting in an asymmetrical beam width curve. Hence, the beam quality did not deteriorate and maintained near-single-mode output despite a slight fluctuation in the time and frequency domain at the output power of 3015 W.

The above results indicate that the GSGDD fiber has a great performance in high power fiber lasers. The TMI threshold of the

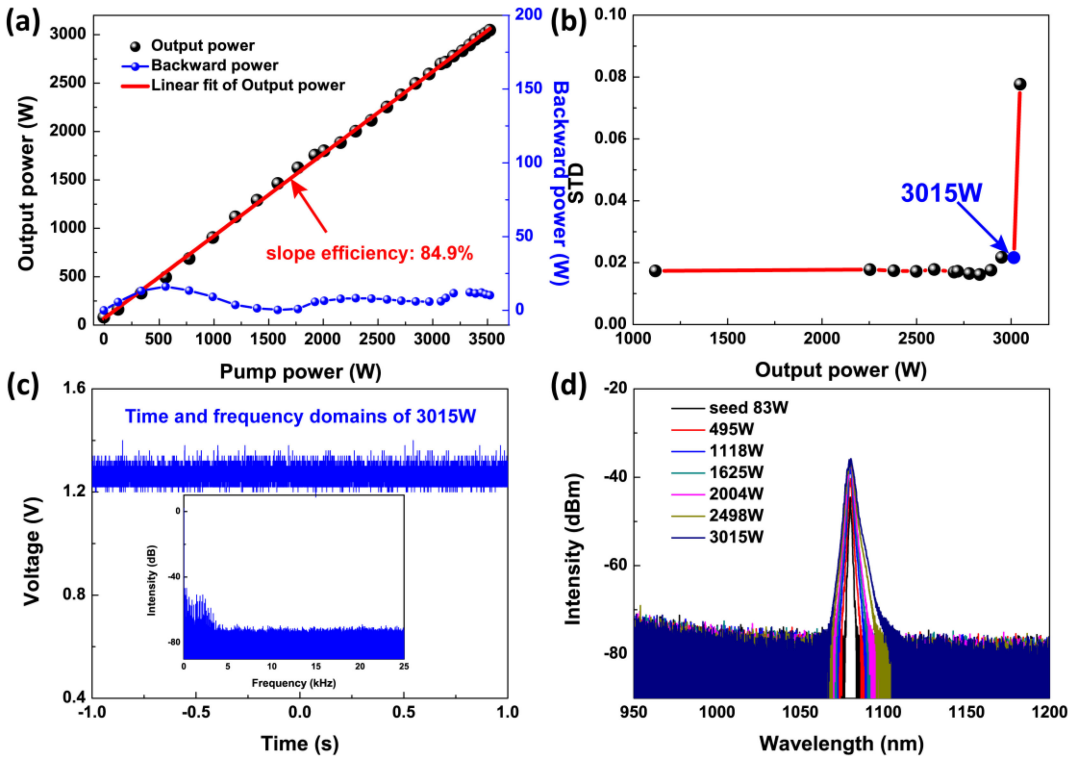

Fig. 6. Experimental results of bidirectional-pumping scheme. (a) Output powers and backward powers at different pump powers; (b) Standard deviations at several output powers; (c) The time and frequency domain at output power of 3015 W; (d) Laser spectrums of several output powers.

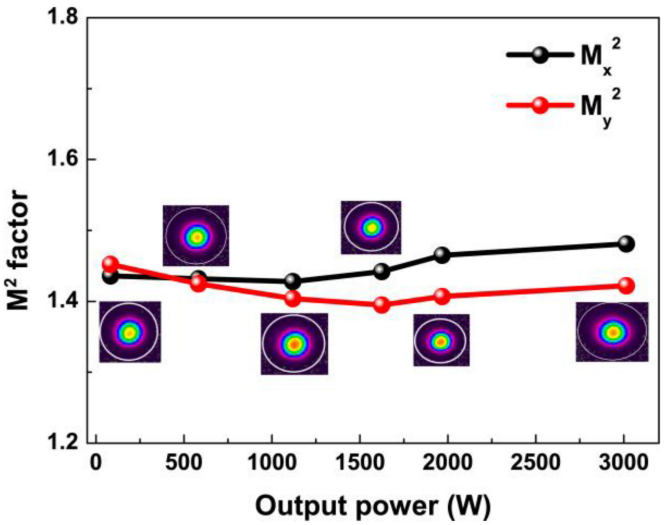

Fig. 7. The beam quality M^2 factors at several output powers.

co-pumping scheme is about 1598 W, which is about 2.23 times and 1.28 times as much as that of the conventional fiber and the confined-doped fiber with the core and inner cladding diameter of ~33 μm and 400 μm, respectively, experimentally reported in Ref. [20]. Firstly, the Gaussian gain dopant profile better matches the FM gain field, making FM easier to be dominant in transverse mode competition and enlarging the gain difference between FM and HOM [23]. Additionally, Ce^{3+} codoping effectively inhibits the photodarkening effect [28],[29], which further mitigates TMI [31]. Finally, lower pump absorption leads to the longer fiber length, which is more beneficial to balance the distribution of heat load [16]. The above points may be the reasons for the high TMI threshold of GSGDD fiber. In terms of beam quality, it may be advantageous for Gaussian-shaped gain dopant profile to accommodate tighter coiling diameter such as 8.5 cm in this experiment and maintain excellent beam quality in power scaling, as predicted in Ref. [22]. Certainly, based on this fiber, the output power and the beam quality we have achieved still have the potential to be promoted. Further optimizing the fiber designs and laser systems, higher power fiber lasers with better beam quality is expected to be achieved. For instance, increasing the number of soot layers to optimize the gain dopant profile, undoped gain dopant near the edge of fiber core is beneficial to reduce HOMs gain, and optimizing the pump wavelength and the injection conditions.

V. Conclusion

To summarize, we have designed and successfully fabricated a GSGDD fiber by MCVD process combined with SDT. The gain dopant profile is well fitted to the Gaussian type, and the RIP is approximate stepped. The core and inner cladding diameter of GSGDD fiber are ~32 μm and ~400 μm, respectively, with a Gaussian width of 16.9 μm. The laser performance of this fiber was verified based on a bidirectional-pumping MOPA setup, obtaining over 3 kW laser output with a slope efficiency of 84.9%. There is no SRS effect with the fiber length of 28 m in the whole experiment. The M^2 factor of 3 kW is ~1.45, while that of seed is ~1.44, invariably maintaining near-single-mode output during power scaling. The results suggest that GSGDD

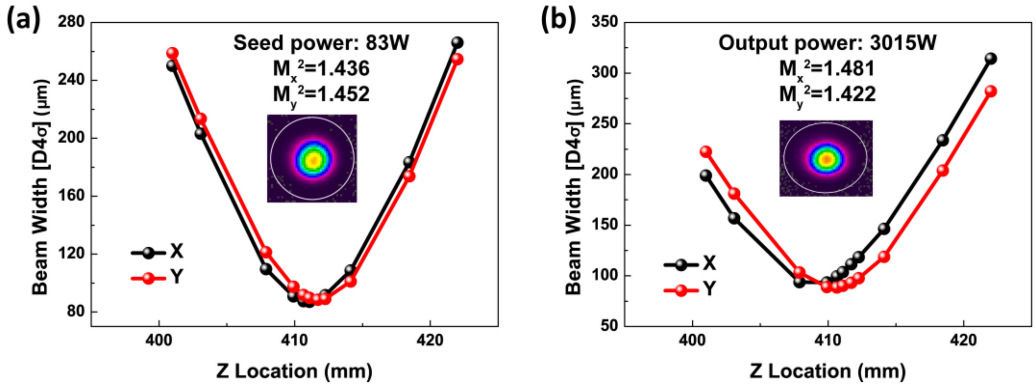

Fig. 8. (a) The beam quality at seed power of 83 W; (b) The beam quality at output power of 3015 W.

fiber has great potential to achieve higher power output with more excellent beam quality, through optimizing fiber design and fabrication and promoting the beam quality of master oscillator.

ACKNOWLEDGMENT

The authors thank Yun Ye, Yinchao Wan, Zhejian Hong and Xiaoyong Xu from National University of Defense and Technology for their assistance during the experiment.

REFERENCES

[1] D. J. Richardson, J. Nilsson, and W. A. Clarkson, "High power fiber lasers: Current status and future perspectives," *J. Opt. Soc. Amer. B*, vol. 27, no. 11, 2010, Art. no. B63.
[2] C. Jauregui, J. Limpert, and A. Tünnermann, "High-power fibre lasers," *Nature Photon.*, vol. 7, no. 11, pp. 861–867, 2013.
[3] C. Codemard, M. N. Zervas, and C. A. Codemard, "High power fiber lasers: A review," *IEEE J. Sel. Top. Quantum Electron.*, vol. 20, no. 5, Sep./Oct. 2014, Art. no. 0904123.
[4] V. Fomin, V. Gapontsev, E. Shcherbakov, A. Abramov, A. Ferin, and D. Mochalov, "100 kW CW fiber laser for industrial applications," *Proc. Int. Conf. Laser Opt. LO*, 2014, Art. no. 3600.
[5] Y. Wang *et al.*, "30/900 Yb-doped aluminophosphosilicate fiber presenting 6.85-kW laser output pumped with commercial 976-nm laser diodes," *J. Lightw. Technol.*, vol. 36, no. 16, pp. 3396–3402, 2018.
[6] L. Quintino, A. Costa, R. Miranda, D. Yapp, V. Kumar, and C. J. Kong, "Welding with high power fiber lasers – A preliminary study," *Mater. Des.*, vol. 28, no. 4, pp. 1231–1237, 2007.
[7] O. Kalisky *et al.*, "The status of high-power lasers and their applications in the battlefield," *Opt. Eng.*, vol. 49, no. 9, 2010, Art. no. 091003.
[8] T. Eidam *et al.*, "Femtosecond fiber CPA system emitting 830 w average output power," *Opt. Lett.*, vol. 35, no. 2, pp. 94–96, 2010.
[9] T. Eidam *et al.*, "Experimental observations of the threshold-like onset of mode instabilities in high power fiber amplifiers," *Opt. Exp.*, vol. 19, no. 14, 2011, Art. no. 13218.
[10] B. Ward, C. Robin, and I. Dajani, "Origin of thermal modal instabilities in large mode area fiber amplifiers," *Opt. Exp.*, vol. 20, no. 10, 2012, Art. no. 11407.
[11] A. V. Smith and J. J. Smith, "Mode competition in high power fiber amplifiers," *Opt. Exp.*, vol. 19, no. 12, 2011, Art. no. 11318.
[12] K. R. Hansen, T. T. Alkeskjold, J. Broeng, and J. Lægsgaard, "Thermally induced mode coupling in rare-earth doped fiber amplifiers," *Opt. Lett.*, vol. 37, no. 12, 2012, Art. no. 2382.
[13] C. Jauregui *et al.*, "On the thermal origin of mode instabilities in high power fiber lasers," in *Fiber Lasers IX Technol. Syst. Appl.*, vol. 8237, Feb. 2012, Art. no. 82370D.
[14] S. Naderi, I. Dajani, T. Madden, and C. Robin, "Investigations of modal instabilities in fiber amplifiers through detailed numerical simulations," *Opt. Exp.*, vol. 21, no. 13, 2013, Art. no. 16111.
[15] R. Tao, P. Ma, X. Wang, P. Zhou, and Z. Liu, "Influence of core NA on thermal-induced mode instabilities in high power fiber amplifiers," *Laser Phys. Lett.*, vol. 12, no. 8, 2015, Art. no. 085101.
[16] A. V. Smith and J. J. Smith, "Increasing mode instability thresholds of fiber amplifiers by gain saturation," *Opt. Exp.*, vol. 21, no. 13, 2013, Art. no. 15168.
[17] H.-J. Otto, A. Klenke, C. Jauregui, F. Stutzki, J. Limpert, and A. Tünnermann, "Scaling the mode instability threshold with multicore fibers," *Opt. Lett.*, vol. 39, no. 9, 2014, Art. no. 2680.
[18] T. Eidam *et al.*, "Preferential gain photonic-crystal fiber for mode stabilization at high average powers," *Opt. Exp.*, vol. 19, no. 9, 2011, Art. no. 8656.
[19] S. Naderi, I. Dajani, J. Grosek, and T. Madden, "Theoretical and numerical treatment of modal instability in high-power core and cladding-pumped raman fiber amplifiers," *Opt. Exp.*, vol. 24, no. 15, 2016, Art. no. 16550.
[20] F. Zhang *et al.*, "Gain-tailored yb/ce codoped aluminosilicate fiber for laser stability improvement at high output power," *Opt. Exp.*, vol. 27, no. 15, 2019, Art. no. 20824.
[21] M. Gong, Y. Yuan, C. Li, P. Yan, H. Zhang, and S. Liao, "Numerical modeling of transverse mode competition in strongly pumped multimode fiber lasers and amplifiers," *Opt. Exp.*, vol. 15, no. 6, 2007, Art. no. 3236.
[22] C. Ye, J. Koponen, T. Kokki, J. Montiel i Ponsoda, A. Tervonen, and S. Honkanen, "Confined-doped ytterbium fibers for beam quality improvement: Fabrication and performance," in *Fiber Lasers IX Technol. Syst. Appl.*, vol. 8237, 2012, Art. no. 823737.
[23] J. R. Marciante, "Gain filtering for single-spatial-mode operation of large-mode-area fiber amplifiers," *IEEE J. Sel. Top. Quantum Electron.*, vol. 15, no. 1, pp. 30–36, Jan. 2009.
[24] J. R. Marciante, R. G. Roides, V. V. Shkunov, and D. A. Rockwell, "Near-diffraction-limited operation of step-index large-mode-area fiber lasers via gain filtering," *Opt. Lett.*, vol. 35, no. 11, 2010, Art. no. 1828.
[25] C. P. Seah, W. Y. W. Lim, and S. L. Chua, "A 4kW fiber amplifier with good beam quality employing confined-doped gain fiber," *Opt. InfoBase Conf. Pap.*, vol. Part F121-, pp. 2–3, 2018.
[26] J. P. Leidner and J. R. Marciante, "Three fiber designs for mitigating thermal mode instability in high-power fiber amplifiers," *Opt. Exp.*, vol. 28, no. 19, 2020, Art. no. 28502.
[27] V. Petit, T. Okazaki, E. H. Sekiya, R. Bacus, K. Saito, and A. J. Ikushima, "Characterization of yb^{3+} clusters in silica glass preforms," *Opt. Mater.*, vol. 31, no. 2, pp. 300–305, 2008.
[28] N. Zhao *et al.*, "Investigation of cerium influence on photo-darkening and photo-bleaching in Yb-doped fibers," *Appl. Phys. A Mater. Sci. Process.*, vol. 122, no. 2, pp. 1–5, 2016.
[29] M. Engholm, P. Jelger, F. Laurell, and L. Norin, "Improved photodarkening resistivity in ytterbium-doped fiber lasers by cerium codoping," *Opt. Lett.*, vol. 34, no. 8, 2009, Art. no. 1285.
[30] Y. Liu *et al.*, "Single transverse mode laser in a center-sunken and cladding-trenched Yb-doped fiber," *Opt. Exp.*, vol. 26, no. 3, 2018, Art. no. 3421.
[31] C. Jauregui, H.-J. Otto, F. Stutzki, J. Limpert, and A. Tünnermann, "Simplified modelling the mode instability threshold of high power fiber amplifiers in the presence of photodarkening," *Opt. Exp.*, vol. 23, no. 16, 2015, Art. no. 20203.